Single phase *a*-plane MgZnO epilayers for UV optoelectronics: substitutional behavior of Mg at large contents

A. Redondo-Cubero,†*[ab] A. Hierro,[b] J.-M. Chauveau,[c] K. Lorenz,[a] G. Tabares,[b] N. Franco,[a] E. Alves[a] and E. Muñoz[b]

High quality 1 μm thick *a*-plane $Mg_xZn_{1-x}O$ layers were produced by molecular beam epitaxy with Mg contents higher than 50%. Resonant Rutherford backscattering spectrometry combined with ion channeling revealed a uniform growth in both composition and atomic order. The lattice-site location of Mg, Zn and O elements was determined independently, proving the substitutional behavior of Mg in Zn-sites of the wurtzite lattice. X-Ray diffraction pole figure analysis also confirms the absence of phase separation. Optical properties at such high Mg contents were studied in Schottky photodiodes.

Introduction

The successful progress of the technology based on wide band gap semiconductors has been driven by considerable efforts towards the achievement of high-quality materials, concerning both the epitaxial growth and the opto-electronic performance. In the last few years, a rising interest has been devoted to the development of ZnO-based devices, because of their particular advantages (availability of bulk substrates and high free exciton binding energy, among others).[1] In novel ZnO optoelectronics, ternary $Mg_xZn_{1-x}O$ compounds have become an essential and active part, allowing band gap engineering and also exhibiting interesting properties towards the achievement of efficient p-type doping.[2,3] Moreover, the accomplishment of UV LEDs based on MgZnO has been demonstrated very recently.[4]

Nevertheless, due to the different stable phases of MgO (rock salt) and ZnO (wurtzite), the potential of these ternary layers is strongly limited by the presence of phase separation for $x \approx 0.4$.[5] Although some works have reported the growth of wurtzite *c*-plane MgZnO layers with $x \approx 0.5$,[6,7] most of the attempts to achieve high Mg contents finally led to cubic structures.[5,8] Actually, the *in situ* work of Takeuchi *et al.* on graded MgZnO films has evidenced the appearance of phase separation for $0.4 < x < 0.6$ in the form of Mg-rich precipitated nanograins.[9]

The large miscibility gap found between MgO and ZnO under thermal equilibrium limits the maximum Mg content achievable by chemical deposition techniques, but it can be partially overcome by using molecular beam epitaxy (MBE), since the growth by MBE can be set far from the alloy equilibrium conditions, the elemental fluxes can be controlled independently, and the oxidation efficiency can be enhanced.[1] In fact, the highest reported Mg contents in $Mg_xZn_{1-x}O$ ($x \approx 0.5$) have been obtained using MBE.[10–12] However, the growth of such epilayers without phase separation is still a challenging issue, especially in the case of non-polar orientations, where crystal quality is still poor. Very few works have reported the growth of *a*-plane MgZnO layers until now, and state-of-the-art films are mainly restricted to low thicknesses and low Mg contents (below 30%). Nevertheless, Takagi and co-workers have mentioned the important role of the growth direction in the transition from the wurtzite to the rock salt phase (appearing normally along the *c*-axis), which can be prevented using appropriate ZnO buffer layers.[11] Therefore, the combination of both an *a*-plane orientation and a ZnO Mg buffer layer might result in a more accurate growth of $Mg_xZn_{1-x}O$ for large x values. In addition, transmission electron microscopy (TEM) and X-ray diffraction (XRD) studies of *a*-plane $Mg_xZn_{1-x}O$ films demonstrated that most of the initial strain is relieved at the first stages of the growth due to a strong anisotropic relaxation.[13,14] Following this approach, Chauveau *et al.* have pointed out the possibility of growing $Mg_xZn_{1-x}O$/ZnO quantum wells ($x \approx 0.2$) without phase separation,[15] which might represent an important breakthrough for future ZnO-based UV optoelectronics.

In this paper, we report the growth of high-quality thick *a*-plane $Mg_xZn_{1-x}O$ epilayers with $x = 0.44$, 0.52, and 0.56. The in-depth composition and crystal quality were measured by resonant Rutherford backscattering spectrometry (RBS) in random and channelling geometries (RBS/C), respectively. RBS/C angular scans were recorded to determine the lattice-site location of Mg, Zn and O atoms, and further verification of the single-phase character was done by XRD pole figures. Finally, standard optical and electrical characterization was performed in Au–MgZnO Schottky photodiodes.

[a]*Instituto Tecnológico e Nuclear, 2686-953 Sacavém, Portugal. E-mail: aredondo@itn.pt*
[b]*Instituto de Sistemas Optoelectrónicos y Microtecnología, Universidad Politécnica de Madrid, E-28040 Madrid, Spain*
[c]*Centre de Recherche sur l'HétéroEpitaxie et ses Applications (CRHEA-CNRS), F-06560 Valbonne Sophia Antipolis, France*
† Previously at Center of Micro-Analysis of Materials, Spain.

Experimental section

A series of ~1 μm thick $Mg_xZn_{1-x}O$ samples were grown on *r*-plane sapphire in a Riber Epineat MBE system equipped with effusion cells for elemental Zn and Mg. Atomic oxygen was supplied *via* an Addon radio-frequency (rf) plasma cell using an rf power. The growth temperature was controlled by a thermocouple located behind the substrate and by an infrared pyrometer. A low temperature ZnO Mg buffer layer was grown and annealed at 600 °C under O flux. This layer is essential to prevent phase separation[11] but, in *a*-plane orientations, it also enhances the initial strain relaxation associated with the large initial misfit along the in-plane [1$\bar{1}$00] direction.[14] The MgZnO epilayer was grown at ~400 °C at a rate of 0.2 μm h^{-1}. The Mg concentration was controlled by changing the flux ratio between the Zn and the Mg elements from 40 to 25. Additional details of the growth conditions for a-ZnMgO/r-sapphire can be found in ref. 12,14 and 15.

RBS/C experiments were performed with a 3.035 MeV ^{4}He beam (1 × 1 mm^2 spot). The probing energy was selected to increase the sensitivity to O (thanks to the nuclear resonance of this element[16,17]) and, simultaneously, to allow certain separation of Zn and Mg signals (needed for the lattice-site analysis). Backscattered ions were detected by a Si barrier detector placed at a scattering angle of 170° (IBM geometry). A 3-axis goniometer was employed to control the crystal position with an accuracy of 0.01°. Aligned and random spectra were simulated using the RBX code.[18]

Further structural characterization by XRD was carried out using a D8Discover diffractometer (Bruker-AXS) with Cu($K_{\alpha 1}$) radiation, an asymmetric 2-bounce Ge(220) monochromator and a scintillation detector. Pole figures were recorded in the bisecting geometry for both (11$\bar{2}$0) and (20$\bar{2}$5) reflections. A large aperture was placed in front of the detector to warrant an acceptance range of $2\theta \pm 5°$.

Results and discussion

RBS/C characterization: composition and crystal quality

Fig. 1 shows the random and ⟨11$\bar{2}$0⟩ aligned RBS/C spectra of the $Mg_{0.52}Zn_{0.48}O$ epilayer, which is representative of the series.

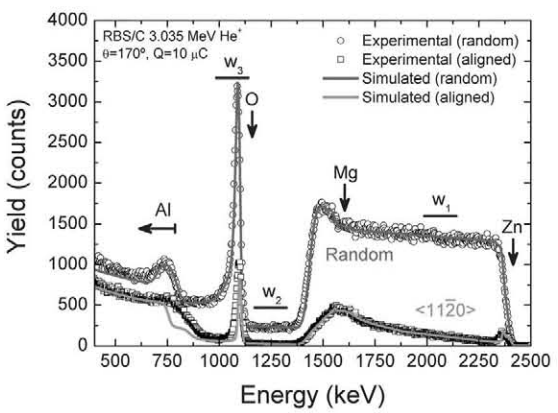

Fig. 1 Random and ⟨11$\bar{2}$0⟩ aligned spectra (circles and squares) of the $Mg_xZn_{1-x}O$ sample with $x = 0.52$ (as derived from simulations, in solid lines). Windows for the lattice-site analysis of Zn (w_1), Mg (w_2) and O (w_3) are displayed.

The composition was extracted from the fitting of the random spectrum. Apart from the rough interface of a few nm (corresponding to the initial stage of the growth), a single-layer model was assumed to simulate the MgZnO layer. In all cases, the simulations show a homogeneous growth, with a constant composition for thicknesses as high as 1 μm. The composition found for the three samples was $x = 0.44(1)$, 0.52(1) and 0.56(1), respectively. These values are comparable and even higher than the highest already reported Mg contents in *c*-plane layers.[6,7]

In order to confirm the crystal quality and single-phase character of the films, quantitative information was also obtained, thanks to the channeling effect[19] along the ⟨11$\bar{2}$0⟩ axis. In particular, the determination of the minimum yield (χ_{min}), defined as the ratio between aligned and random yields, gives a direct measure of the crystal quality, and it can be analyzed for different depths and elements depending on the selected energy window. The aligned spectra of the samples show $\chi_{min} = 3.2(2)\%$, 4.2(3)%, and 5.4(4)%, for the compositions $x = 0.44$, 0.52 and 0.56, respectively, this calculation being done for the Zn signal close to the surface. These values demonstrate the excellent crystal quality of the samples, also confirmed by XRD measurements (discussed later on). Remarkably, these values are close to those already reported on *c*-plane MgZnO films (with $\chi_{min} \approx 5\%$).[20] As shown in Fig. 1, the good quality of the layers is also preserved with depth, and a significant rise of χ_{min} is only visible for ions reaching the buffer layer (energies between 1500 and 1700 keV). This feature is characteristic of many systems grown epitaxially on sapphire, and reflects the defect formation induced by the lattice mismatch at the beginning of the growth.[21]

RBS/C angular scans: lattice-site location

In addition to the information related with the crystal quality, the characteristic channelling dip of the angular scans can be used to identify the substitutional behaviour of the different atoms in the lattice and to detect phase separation.[22] This is generally verified by probing different crystallographic directions,[19] although some specific features of the channeling dips are often used as fingerprints of lattice sites. In particular, the asymmetric shadowing effect for positive or negative incident angles is a well-known phenomenon that leads to unambiguous lattice site location in mixed semiconductors.[23,24]

Fig. 2a and b compare the lattice projections of the two axes selected for the RBS/C angular scans. The scan orientations are marked in dashed lines. Because of the alignment of the atomic rows in these scans, the shadowing effect results in asymmetric dips in the ⟨11$\bar{2}$0⟩ axis and symmetric dips in the ⟨1$\bar{1}$00⟩ axis, which was also verified with Monte Carlo simulations using the FLUX code.[25] Fig. 2c and d show ⟨11$\bar{2}$0⟩ and ⟨1$\bar{1}$00⟩ scans for the $Mg_{0.52}Zn_{0.48}O$ sample. The Mg, Zn and O signals were analyzed using the three windows defined in Fig. 1. Note that w_1 (Zn) and w_2 (Mg) correspond to the same depth inside the layer to allow the direct comparison of χ_{min}. Due to the overlap of Mg and O signals, the Mg background was extrapolated using w_2 and then subtracted from w_3 for the integration of the O dip.

As it is clear from Fig. 2c, the Zn-site remains quite symmetric, while the O-site shows a notorious shoulder at $\theta \approx -0.6°$ and the extra minimum at $\theta \approx 0.6°$. These characteristics identify both sites and are in correspondence with the lattice asymmetry

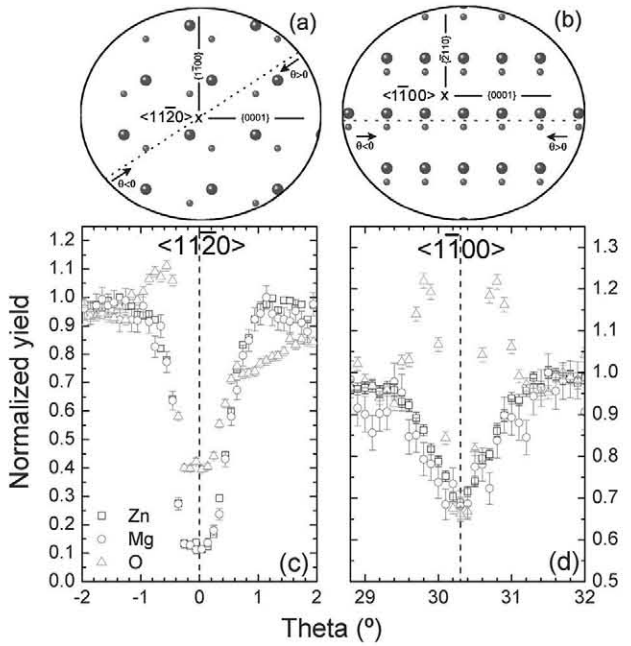

Fig. 2 (a and b) Lattice projections along the $\langle 11\bar{2}0\rangle$ and $\langle 1\bar{1}00\rangle$ axes of a wurtzite crystal (dashed lines show the scan directions). (c and d) Experimental angular scans across $\langle 11\bar{2}0\rangle$ and $\langle 1\bar{1}00\rangle$ axes for the $Mg_{0.52}Zn_{0.48}O$ sample. The Mg dip completely overlaps with the Zn one in both directions, indicating its substitutional behavior.

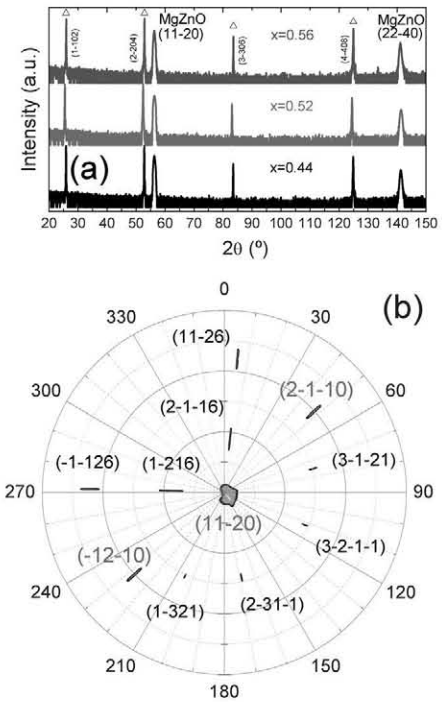

Fig. 3 (a) XRD $2\theta/\omega$ scans of $Mg_xZn_{1-x}O$ samples with $x \approx 0.5$ where only wurtzite peaks are detected (triangles mark sapphire reflections). (b) Pole figure around the $(11\bar{2}0)$ plane in the $Mg_{0.52}Zn_{0.48}O$ sample showing the absence of cubic phases. Poles marked in red represent wurtzite MgZnO, while poles in black are from sapphire.

discussed before (note that the radius of the shadow cone scales with atomic mass,[19] so the Zn dip is less affected by the asymmetry than O). The Mg dip depicted in Fig. 2c is in perfect agreement with the Zn-site. This fact, verified in the three samples, is a conclusive proof of the substitutional behavior of Mg in the wurtzite lattice. Furthermore, the same behavior was verified in the $\langle 1\bar{1}00\rangle$ axis, where Mg and Zn dips fit exactly. In this scan both Zn and O sites are expected to be symmetric (see Fig. 2b), but the O signal exhibits prominent shoulders useful for the identification of the O-site.

XRD patterns and pole figures

Fig. 3a shows XRD $2\theta/\omega$ scans for all samples. Apart from the sapphire reflections associated with the $\{1\bar{1}02\}$ planes, only $(11\bar{2}0)$ and $(22\bar{4}0)$ peaks from MgZnO layers were detected (at $2\theta = 56.3°$ and 141.1°). FWHM from $(11\bar{2}0)$ ω rocking curves was obtained with the X-ray beam parallel to the in-plane c-axis (note that FWHM depends on the orientation[15]). The FWHM values range between 0.57° and 0.68°, confirming the good crystal quality previously observed by RBS/C, although they are larger than that of a reference a-plane ZnO sample (FWHM = 0.29°). Since $2\theta/\omega$ scans are not sufficient to rule out completely the presence of cubic ternary phases, pole figures were recorded as described in the Experimental section. Fig. 3b shows the pole figure of the $Mg_{0.52}Zn_{0.48}O$ sample for $2\theta = 56.3°$ corresponding to the $(11\bar{2}0)$ planes. Due to the large acceptance angle used, sapphire $\{2\bar{1}\bar{1}6\}$, $\{3\bar{1}2\bar{1}\}$, $\{3\bar{1}\bar{2}2\}$, and $\{10\bar{1}8\}$ reflections were also detected at $2\theta = 57.5°$, 59.8°, 61.2°, and 61.3°, respectively. Apart from these reflections, only wurtzite poles were identified. Additional pole figures centered at $2\theta = 36.9°$, 42.9°, and 144.3°, corresponding to (111), (200), and (333) reflections of potential cubic MgZnO inclusions, were recorded. Again, only sapphire reflections were found, ruling out the presence of phase separation, in agreement with RBS/C data.

Optical response

Au–$Mg_xZn_{1-x}O$ Schottky photodiodes were fabricated for the three mentioned samples (and the additional a-plane ZnO reference) with a 10 nm semitransparent contact (200 μm

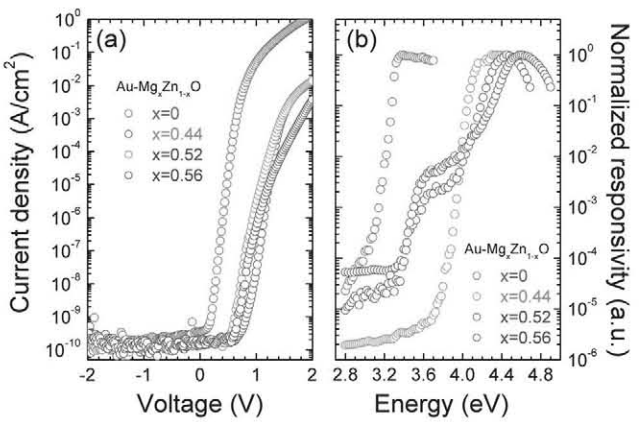

Fig. 4 (a) I–V characteristics of the Au–MgZnO photodiodes measured in the dark. (b) Normalized spectral response at −1.5 V for different compositions. The results for a-plane ZnO are also included as a reference.

diameter).[26] Fig. 4 shows the dark current–voltage (I–V) characteristics and the normalized responsivity determined for such photodetectors. An excellent rectifying behaviour of the diodes was confirmed, even for the highest Mg contents. Correspondingly, the absorption edge shifts towards high energies (up to 4.6 eV for $x = 0.56$), the broad feature at 3.4–3.6 eV being ascribed to the ZnO Mg buffer layer. Although the total responsivity was found to decrease with x, the high UV/VIS rejection ratio (~4 to 6 orders of magnitude) demonstrates their potential for application in UV detectors.

Conclusions

In summary, we have shown that high quality a-plane $Mg_xZn_{1-x}O$ epilayers with $x > 0.5$ can be grown without phase separation. The substitutional behaviour of Mg in Zn-sites was confirmed by the RBS/C scans, and XRD pole figures demonstrated the absence of cubic inclusions. The results on fabricated photodiodes show that MgZnO-based UV optoelectronic devices may be successfully developed using non-polar planes.

Acknowledgements

We acknowledge support by grants TEC2008-04718, PIB2010JP-00279 and TEC2011-28076-C02-01 (MICINN, Spain), PTDC/CTM/100756/2008 and SFRH/BPD/74095/2010 (FCT, Portugal). We also thank the support from the Centre of Micro-Analysis of Materials, and fruitful discussions with Dr V. Darakchieva and Prof. P.J.M. Smulders.

References

1 Ü. Özgür, Y. I. Alivov, C. Liu, A. Teke, M. A. Reshchikov, S. Doğan, V. Avrutin, S.-J. Cho and H. Morkoç, *J. Appl. Phys.*, 2005, **98**, 041301.
2 H. Kato, T. Yamamuro, A. Ogawa, C. Kyotani and M. Sano, *Appl. Phys. Express*, 2011, **4**, 091105.
3 S. Akasaka, K. Nakahara, A. Tsukazaki, A. Ohtomo and M. Kawasaki, *Appl. Phys. Express*, 2010, **3**, 071101.
4 K. Nakahara, S. Akasaka, H. Yuji, K. Tamura, T. Fujii, Y. Nishimoto, D. Takamizu, A. Sasaki, T. Tanabe, H. Takasu, H. Amaike, T. Onuma, S. F. Chichibu, A. Tsukazaki, A. Ohtomo and M. Kawasaki, *Appl. Phys. Lett.*, 2010, **97**, 013501.
5 S. Choopun, R. D. Vispute, W. Yang, R. P. Sharma, T. Venkatesan and H. Shen, *Appl. Phys. Lett.*, 2002, **80**, 1529.
6 W. I. Park, G. C. Yi and H. M. Jang, *Appl. Phys. Lett.*, 2001, **79**, 2022.
7 H. Tanaka, S. Fujita and S. Fujita, *Appl. Phys. Lett.*, 2005, **86**.
8 J. Chen, W. Z. Shen, N. B. Chen, D. J. Qiu and H. Z. Wu, *J. Phys.: Condens. Matter*, 2003, **15**, L475.
9 I. Takeuchi, W. Yang, K.-S. Chang, M. A. Aronova, T. Venkatesan, R. D. Vispute and L. A. Bendersky, *J. Appl. Phys.*, 2003, **94**, 7336.
10 Y. N. Hou, Z. X. Mei, Z. L. Liu, T. C. Zhang and X. L. Du, *Appl. Phys. Lett.*, 2011, **98**, 103506.
11 T. Takagi, H. Tanaka and S. Fujita, *Jpn. J. Appl. Phys., Part 2*, 2003, **42**, L401.
12 J.-M. Chauveau, J. Vives, J. Zuniga-Perez, M. Laügt, M. Teisseire, C. Deparis, C. Morhain and B. Vinter, *Appl. Phys. Lett.*, 2008, **93**, 231911.
13 J.-F. Carlin and M. Ilegems, *Appl. Phys. Lett.*, 2003, **83**, 663.
14 J.-M. Chauveau, P. Vennéguès, M. Laügt, C. Deparis, J. Zuniga-Perez and C. Morhain, *J. Appl. Phys.*, 2008, **104**, 073535.
15 J.-M. Chauveau, M. Laügt, P. Vennéguès, M. Teisseire, B. Lo, C. Deparis, C. Morhain and B. Vinter, *Semicond. Sci. Technol.*, 2008, **23**, 035005.
16 J. A. Leavitt, L. C. McIntyre, Jr, M. D. Ashbaugh, J. G. Oder, Z. Lin and B. Dezfouly-Arjomandy, *Nucl. Instrum. Methods Phys. Res., Sect. B*, 1990, **44**, 260.
17 A. Redondo-Cubero, M. Vinnichenko, M. Krause, A. Mücklich, E. Muñoz, A. Kolitsch and R. Gago, *J. Appl. Phys.*, 2011, **110**, in press.
18 E. Kótai, *Nucl. Instrum. Methods Phys. Res., Sect. B*, 1994, **85**, 588.
19 L. C. Feldman, J. W. Mayer and S. T. Picraux, *Materials Analysis by Ion Channelling*, Academic Press, New York, 1982.
20 A. K. Sharma, J. Narayan, J. F. Muth, C. W. Teng, C. Jin, A. Kvit, R. M. Kolbas and O. W. Holland, *Appl. Phys. Lett.*, 1999, **75**, 3327.
21 A. Redondo-Cubero, R. Gago, F. González-Posada, U. Kreissig, M.-A. di Forte Poisson, A. F. Braña and E. Muñoz, *Thin Solid Films*, 2008, **516**, 8447.
22 A. Redondo-Cubero, K. Lorenz, R. Gago, N. Franco, M.-A. di Forte Poisson, E. Alves and E. Muñoz, *J. Phys. D: Appl. Phys.*, 2010, **43**, 055406.
23 J. U. Andersen, N. G. Chechenin and Z. Z. Hua, *Appl. Phys. Lett.*, 1981, **39**, 758.
24 T. Haga, H. Suzuki, M. H. Rashid, Y. Abe and A. Tanaka, *Appl. Phys. Lett.*, 1988, **52**, 200.
25 P. J. M. Smulders and D. O. Boerma, *Nucl. Instrum. Methods Phys. Res., Sect. B*, 1987, **29**, 471.
26 G. Tabares, A. Hierro, J. M. Ulloa, A. Guzman, E. Muñoz, A. Nakamura, T. Hayashi and J. Temmyo, *Appl. Phys. Lett.*, 2010, **96**, 101112.